Pectoral Fin Design and Swimming Performance: Testing Thrust and Efficiency Models with Structure and Behavior of Living Fishes.

Mark W. Westneat
Field Museum of Natural History
Department of Zoology, 1400 S. Lake Shore Drive, Chicago IL 60605, mwestneat@fmnh.org
Jeffrey A. Walker
University of Southern Maine
Department of Biology, 96 Falmouth St., Portland ME 04103, walker@usm.maine.edu

Abstract

Fin-based propulsion systems perform well for both efficient cruising and high maneuverability in fishes, making them good models for propulsors of autonomous underwater vehicles. Labriform locomotion in fishes is actuated by oscillation of the paired pectoral fins. We used a computer simulation to compare the mechanical performance of rowing and flapping appendages across a range of speeds. Flapping appendages proved to be more mechanically efficient than rowing appendages at all swimming speeds, suggesting that animals that frequently engage in locomotor behaviors that require energy conservation should employ a flapping stroke. The lower efficiency of rowing appendages across all speeds begs the question, why does rowing occur at all? Large forces are necessary for maneuvering behaviors such as accelerations, turning, and braking, which suggests that rowing should be found in slow swimming animals that frequently maneuver. The predictions of the model are supported by observed patterns of behavioral variation among rowing and flapping vertebrates. We found a close association between fin design, including both static morphology and dynamic motion, and steady swimming performance in four species of the family Labridae (*Cirrhilabrus rubripinnis*, *Pseudocheilinus octotaenia*, *Gomphosus varius*, and *Halichoeres bivittatus*. A general protocol for pectoral fin morphometrics is proposed and used to generate a set of functionally relevant parameters including aspect ratio, fin chords, and distribution of areas on the fin surface. Aspect ratio ranged from 1.5 to 3.5 in the 4 species. Fin chord lengths and the area distribution from base to tip characterize fins on the continuum from high aspect ratio wing-like fins to low aspect ratio paddle-like fins. Trends in kinematics observed across all four species were increased frequency and stroke angle with increasing swimming speed. *G. varius* and *C. rubripinnis* had significantly more vertical stroke planes than their respective close relatives, *H. bivittatus* and *P. octotaenia*, reflecting a gap between a flapping vs. a rowing strategy. As predicted by a virtual model of rowing vs. flapping appendages, the species with wing-shaped fins and flapping stroke shapes were able to achieve and maintain higher pectoral-fin-powered speeds than the species with paddle-shaped fins and rowing stroke shapes. Labriform propulsion can have comparable performance to that of body-caudal fin swimmers of similar size. AUV designs should incorporate fin shape variability and should mimic fin stroke kinematics of fishes carefully to achieve efficient thrust and maneuverability. Funded by ONR N00014-99-0184.

Introduction

There is considerable research interest focused on the design, mechanics, and hydrodynamics of animal propulsors due to the potential relevance of efficient animal designs for practical applications in underwater vehicle technology. The pectoral fins of fishes (paired fins on the shoulder girdle) have been shown to provide efficient locomotion in coral reef fishes over a wide range of speeds (Walker and Westneat, 2000, 2001). Swimming performance (speed endurance tests for fishes) show that pectoral propulsors are capable of generating thrusts that can power speeds up to 10 body lengths/second in some species (Walker and Westneat, 2001). In addition, these species are highly maneuverable in complex three-dimensional reef habitats. Effici-

ency, speed performance and maneuverability are key aspects of pectoral locomotion that make reef fishes an appropriate model system for underwater vehicle technology. This paper describes research on propulsor designs and swimming performance in several species of reef fish, and tests predictions of hydrodynamic theory by using a computer simulation to compare the mechanical performance of rowing and flapping appendages across a range of speeds.

Breder (1926) recognized two modes of oscillatory pectoral fin propulsion, which he called rowing and flapping. Rowing is a largely fore-aft movement in which the pectoral fins are brought “forward almost edgewise and [forced] back broadside." By contrast, flapping is a largely dorsoventral fin motion. Rowing and flapping are not unique to fishes but occur in a diverse array of animal taxa (Vogel, 1994; Walker and Westneat 2000, 2001). The repeated evolution of rowing and flapping begs the question, why do some animals row while others flap? Walker & Westneat (2000) used a computer simulation to model the performance consequences of rowing and flapping and found that a flapping stroke not only generates more thrust per fin beat at high speeds, as found by Vogel (1994), but also does work with much higher mechanical efficiency at all speeds. Consequently, a flapping geometry should be the preferred motion for behaviors requiring conservation of energy. In contrast, the rowing stroke generates higher thrust over a half-cycle (the power stroke) and should be the preferred motion for maneuvering behaviors requiring large forward accelerations, backward accelerations or lateral turns.

The hypothesis that animals that flap can swim more efficiently than animals that row has been explored in numerous studies on the swimming energetics of rowing or flapping turtles, birds, and mammals. We explored the hypothesis that the geometry of fin motion is causally associated with swimming efficiency by comparing swimming endurance within two pairs of closely related species of wrasse (Labridae). Labrids are an extremely diverse and species-rich family of marine fishes that are both common and conspicuous on all tropical coral reefs. The geometry of fin motion within labrids spans a continuum between rowing and flapping extremes. Initial, qualitative observations suggested that within each of the pairs of species that we studied, at the speeds generally observed in a small aquarium, one member was more at the rowing end of the continuum while the other was more at the flapping end.

Theoretical considerations suggest that rowing and flapping should be associated with very different optimal fin planforms. The optimal shape of a rowing fin is a distally flared paddle (Blake, 1979). This design maximizes the region of the fin that contributes to thrust and minimizes the region of the fin that contributes to drag. In contrast, to reduce the relative loss of energy at the fin tips, flapping pectoral fins should taper near the tip and present relatively high aspect ratios (Vogel, 1994).

Using a theoretical model of fin thrust and efficiency, we examined the relationship between fin shape and stroke mechanics. The goals of this study were (1) present simulation results for a theoretical model of fin function, (2) quantify fin shape differences among species, (3) quantify the degree to which a species rows or flaps its fins, (4) measure swimming endurance in each species, and (5) test the hypothesis that fin shape, kinematics of fin motion, and swimming ability are causally related. Specifically, we expected that fishes with high pectoral-fin-powered endurance should oscillate high aspect ratio, distally tapering fins along a steep stroke plane.

Simulations of Rowing and Flapping

To explore the efficiency of rowing and flapping appendages of different shapes, we used a simulation experiment to measure the affects of dynamic shape on the mechanical performance of an oscillating appendage. A quasi-steady blade-element model that accounted for unsteady phenomena such as added mass effects (Daniel 1984), dynamic stall (Dickinson & Götz 1993; Ellington *et al*. 1996), and the cumulative Wagner effect (Dickinson 1994; Dickinson & Götz 1996; Dickinson *et al*. 1999) was used to estimate two performance variables for the oscillating appendage: the mean thrust over a full and half stroke cycle and the mechanical efficiency of doing work on the fluid.

Each appendage was modeled as a rectangular plate that twisted along its length and

oscillated with simple harmonic motion at a constant amplitude of 60° (Walker and Westneat, 2000), a typical value for fishes that swim with pectoral fins (Blake 1979; Walker & Westneat 1997; Webb 1973). The appendages oscillated around the flapping axis, which had an angle, β, relative to the free stream. β was 90° for the rowing appendage and 0° for the flapping appendage.

Appendages twisted around the pitching axis giving each element an instantaneous pitch, θ, relative to the flapping axis. The flapping appendage twisted about its leading edge with simple harmonic motion (Figure 1). We used two different kinematic models of the recovery stroke for the rowing appendage. For one, the rowing appendage twisted about its trailing edge to attain a feathered orientation (θ ~ -90°) during the fore (recovery) stroke and a broadside orientation (θ = 0°) during the backward (power) stroke. We allowed the rowing appendage to rotate quickly into its feathered or broadside orientation by confining twisting to the first third of the each stroke (Figure 1). For the second model, we allowed the entire span of the appendage to feather (θ = -90°) throughout the recovery stroke.

Dumb coefficients. Blade-element models divide a propulsive structure along its span into a series of blade elements and estimate the force balance on an element using force passing over the element. The basic assumptions of a blade-element model are discussed in Blake (Blake 1979). Previous blade-element models of paired-appendage aquatic propulsion used force coefficients (Hoerner 1958) that reflect the time-averaged normal force on the appendage oriented in a uniform velocity flow at a constant angle of attack (Blake 1979; Blake 1985; Fish 1984; Gal & Blake 1988; Hui 1988; Morris *et al*. 1985). The force on a hydrofoil is not only a function of the its angle of attack but also of its history of motion. Force coefficients are ignorant of their history. In this study, we attempted to model historical effects by using empirically derived lift and drag coefficients measured from root-oscillating plates at Re = 192 (Dickinson *et al*. 1999) and modifying the coefficients by the Wagner function.

The experimental Re of 192 is near the lower bound of the range of Re in which animals both row and flap but we do not have equivalent experimental data at higher Re. For flat plates translating in a uniform flow at a constant angle of attack, force coefficients are fairly constant for 1000 < Re < 100,000 (Hoerner 1958). Below Re = 10, lift coefficients rise slightly but drag coefficients rise sharply (Thom & Swart 1940). Substitution of the normal force coefficients on a flat plate in a steady flow for Re > 1000 (Hoerner 1958) results in the same performance patterns as occur with the lower Re data.

The use of coefficients from oscillating plates accounts for dynamic stall, a phenomenon that increases the normal force on plates translating at moderate to high attack angles due to the presence of an attached vortex on the downstream surface of the airfoil (Kuethe & Chow 1986). The Wagner function accounts for the Wagner effect, a phenomenon that decreases the normal force on impulsively starting plates due to the delay in the generation of circulation (Fung 1993). Dickinson (Dickinson 1994; Dickinson & Götz 1993) showed that dynamic stall overwhelms the Wagner effect if the preceding stroke was at a low attack angle (as in rowing) while the Wagner effect overwhelms the effects of dynamic stall if the preceding stroke was at an intermediate attack angle (as in flapping).

The model. We modeled both circulatory forces resulting from velocity differences on opposing sides of the appendage and added mass forces resulting from the acceleration of a mass of fluid. Circulatory thrust (dT_c), circulatory lift (dL_c), added mass thrust (dT_a), and added mass lift(dL_a) per unit span were computed by (see Fung 1993 and DeLaurier 1993).

$$dT_c = (-dF_n\sin\theta + dF_x\cos\theta)\cos\beta - (dF_n\cos\theta + dF_x\sin\theta)\sin\beta\sin\gamma \quad (1)$$

$$dL_c = (dF_n\cos\theta + dF_x\sin\theta)\cos\beta\sin\gamma + (-dF_n\sin\theta + dF_x\cos\theta)\sin\beta \quad (2)$$

$$dT_a = dF_a\sin\theta\cos\beta + dF_a\cos\theta\sin\beta\sin\gamma \quad (3)$$

$$dL_c = -dF_a\cos\theta\cos\beta\sin\gamma + dF_a\sin\theta\sin\beta \quad (4)$$

where γ is the positional angle of the appendage with 0° up or back against the body. dF_a, the added mass force per unit span, was estimated as $dFa = 1/4\rho\pi c^2 v'_n$, where c is

chord length and v'_n is the first derivative of the normal velocity component of the chord relative to the water,

$$v_n = h' \cos\theta + U_n \sin(\theta + \beta) \pm 1/2 c\theta' \quad (5)$$

where U_n is the flow normal to the span and is found by

$$U_n = U(1 - |\cos\gamma|\sin\beta) \quad (6)$$

The ± in eq. (5) is positive for the flapping fin, which rotates about the leading edge, and negative for the rowing fin, which rotates about the trailing edge. h' is the tangential velocity of a fin element due to fin oscillation. The normal force per unit span was estimated by

$$dF_n = -dT^* \sin\alpha + dL^* \cos\alpha \quad (7)$$

where dL^* and dT^* are the components of the circulatory force normal to and parallel with the local stream. α, the hydrodynamic angle of attack, was found by $\alpha = \pm\tan^{-1}(v_n/v_x)$ where the ± takes the sign of v_x, the chordwise velocity of the section relative to the fluid

$$v_x = -h' \sin\theta + U_n \sin(\theta + \beta) \quad (8)$$

dL^* and dT^* were estimated by

$dL^* = 1/2\rho c(v_x^2 + v_n^2)\phi C_L$ and

$dT^* = 1/2\rho c(v_x^2 + v_n^2)\phi C_D$.

The lift and drag coefficients are from Dickinson et al., 1999.

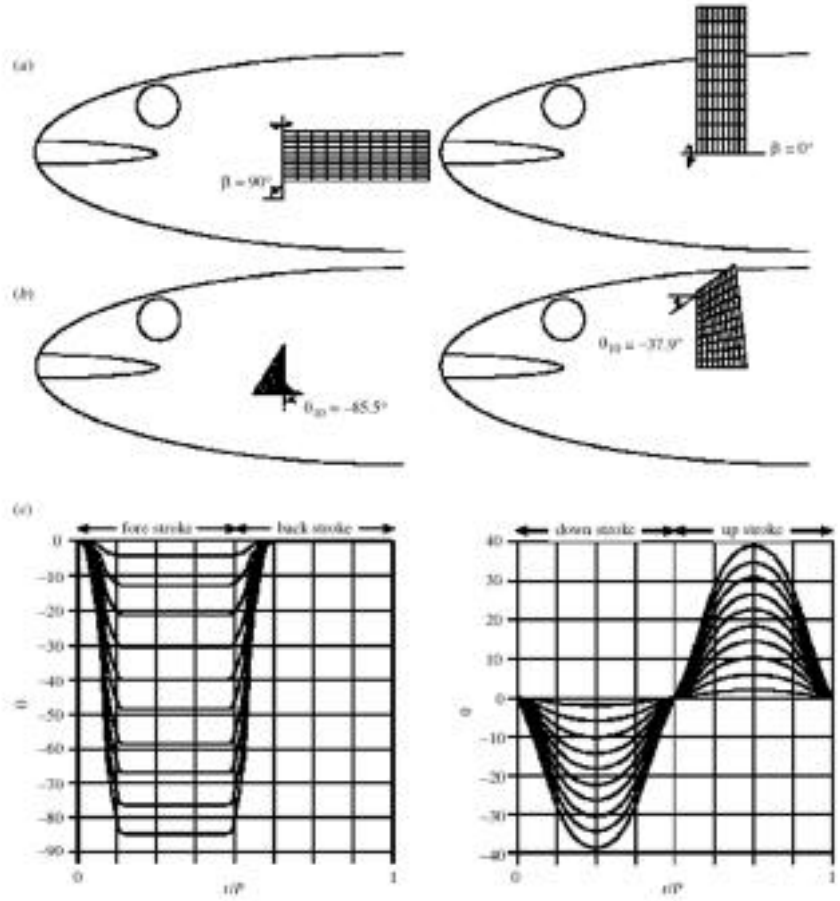

Figure 1. Dynamic shape of oscillating appendage. (*a*) *b* was 90° for the rowing appendage and 0° for the flapping appendage. Oscillation started from a position that was either back (rowing) or straight up (flapping) with no twist. The most distal element is shaded. (*b*) Appendages dynamically twisted around the pitching axis giving each element an instantaneous pitch, θ, which is shown for the most distal element at its maximum negative pitch. (*c*)θ, for the ten blade elements throughout the stroke cycle. The abcissa is time standardized by the stroke Period.

The variable ϕ, an approximation of the Wagner function, was found by $\phi = 1 - 2/(4+\tau)$ (Fung 1993), where τ is the number of semichords traveled during the stroke. For the rowing strokes, or the flapping strokes in which the Wagner effect was ignored, ϕ was set to unity (see above). The chordwise force per unit span was estimated by $dF_x = 1/2\rho c v_x^2 C_{sf}$, where C_{sf} is the coefficient of skin friction drag on the element, $C_{sf} = 1.33/\sqrt{\mathrm{Re}}$ (Hoerner 1958). The input power per unit span, due to both circulatory and added mass forces, was estimated by $dP = dP_c + dP_a$ where

$$dP_c = dF_n(h'\cos\theta \pm 1/2c\theta') + dF_x h'\sin\theta \quad (9)$$

$$dP_a = -dF_a(h'\cos\theta \pm 1/2c\theta') \quad (10)$$

The $\pm$ is positive for the flapping fin and negative for the rowing fin. Thrust, lift and input power were summed across all elements and time increments, multiplied by two to reflect both appendages, and divided by the number of time increments to give mean values. We assumed the appendage worked to accelerate the added mass of water and therefore always used the absolute value of dP_a.

The simulation. As an initial exploration, we ran the model for the rowing and flapping appendages for a variety of oscillation frequencies and forward speeds. In these runs, we computed the mechanical efficiency, η, as a function of reduced frequency. η was found by

$$\eta = T_{avg}U/P_{avg} \quad (11)$$

where T_{avg} and P_{avg} are the mean thrust and mean input power over the full cycle and U is the forward speed of the animal. The reduced frequency, $k = \omega C/2U$, where ω is circular frequency and C is the mean chord, is a measure of the unsteadiness of the flow velocity over the appendage throughout the stroke. For these simulations, we used an appendage with a 3 cm semispan (appendage length) and 1 cm chord, which is about the size of a pectoral fin of an adult bird wrasse (Walker & Westneat 1997).

We also wanted to measure η and T as a function of forward speed. For the runs measuring η, we iterated the model, incrementally increasing the stroke frequency by 0.001 Hz, until a frequency was reached in which T balanced the drag on the body. For this drag, we used the theoretical drag on a body of revolution with a length of 15 cm and a radius of $\sqrt{8}$ cm (Hoerner 1958). Again, these dimensions are about the size of the body of a bird wrasse (Walker & Westneat 1997). The results of our analysis are largely independent of the scale of the appendage and body. dF_x is scale dependent but remains small relative to dF_n in the size range of adult aquatic vertebrates. The normal force coefficient on a flat plate in a steady flow is largely independent of scale at Re > 1000 (Hoerner 1958), which is about the lower end of the range of Re for an oscillating appendage of adult swimming vertebrates and large invertebrates.

At each speed and stroke frequency, η of the flapping fin was computed for all twist amplitudes that resulted in a maximum pitch between $\pm 1°$ and $\pm 90°$ (in increments of 1°) for the distal element of the appendage. For the rowing fin, all twist amplitudes that resulted in a maximum recovery stroke pitch between -90° and -150° (in increments of 1°) for the distal element were computed. We held the pitch of the distal element following the supination at the beginning of the power stroke at a constant 0° (Figure 1). For both rowing and pitching fins, the magnitude of the pitch amplitude that maximized either η or average thrust was chosen for the comparisons.

Simulation Results. The geometry of the recovery stroke greatly influenced the mechanical performance of a rowing appendage (Figure 2). Peak η was 0.51 at k = 0.24 for the feathered rowing appendage but only 0.09 at k = 0.64 for the twisted rowing appendage. The flapping appendage, with a peak η = 0.59 at k = 0.18, oscillated with higher η than the rowing appendage at all k (Figure 2*a*).

For the body simulated here, the flapping appendage generated the necessary force to balance body drag with higher η at all swimming speeds (Figure 2*b*) except the lowest (0.25 BL•s^{-1}). For the flapping fin, η increased steeply with swimming speed, from 0.2 at 0.25 BL•s^{-1} to 0.4 at 6 BL•s^{-1}. Again, performance of the rowing appendage depended on the geometry of the recovery stroke. η decreased from 0.20 at 0.25 BL•s^{-1} to 0.14 at 6 BL•s^{-1} for the feathered rowing appendage and from 0.011 at 0.25 BL•s^{-1} to 0 0.006 at 6 BL•s^{-1} for the twisted rowing

appendage.

Over the entire stroke cycle, the twisted rowing appendage generated more thrust than the flapping appendage only at slow speeds while the feathered rowing appendage generated more thrust than the flapping appendage over much of the speed range (Figure 2*c*). Over the power stroke, mean thrust of either rowing appendage greatly exceeded that for the flapping appendage at all speeds (Figure 2*d*).

Evaluation and uses of the model. The goal of this simulation experiment was to measure the effect of appendage motion (rowing or flapping) on the mechanical performance of an oscillating appendage by holding constant the effects of other variables that potentially influence performance, such as fin shape, amplitude, and phase differences between pitching and oscillation. Our two rowing models should set upper and lower bounds on the mechanical performance of real limbs. The experiment has three important results. First, these are the first direct comparisons of η for rowing and flapping appendages oscillating in the same hydrodynamic environment. We compare our model with experimental data and find good agreement. Second, flapping appendages are more mechanically efficient than rowing appendages at all speeds. We discuss the behavioral consequences of this energetic difference. Finally, at slow speeds, flapping appendages are more efficient but rowing appendages generate more thrust. Large thrust, in turn, facilitates maneuverability. We suggest that the performance trade-off at slow speeds explains the presence of rowing in some aquatic vertebrates, especially fishes.

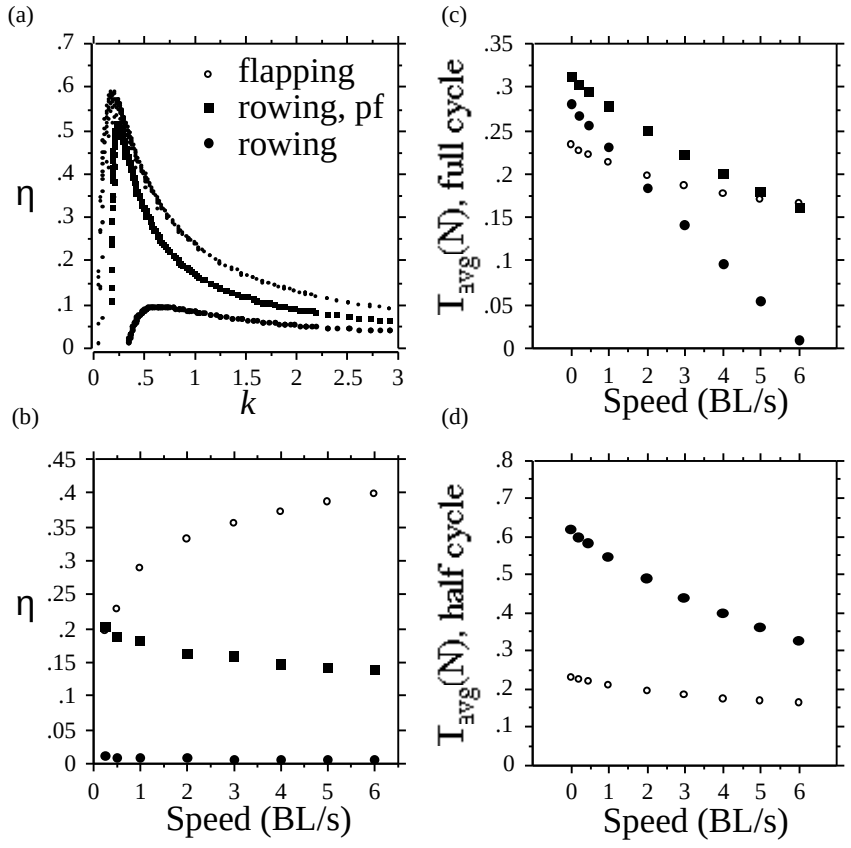

Figure 2. Mechanical efficiency, η, and mean thrust, T, of paired rowing or flapping appendages. (a) η as a function of reduced frequency. (b) η as a function of speed. (c and d) Mean thrust over the (c) full cycle and (d) power stroke (up stroke for flapping appendage and back stroke for rowing appendage). Mean thrust was computed for simulated appendages that oscillated at a frequency of 10 Hz. The dynamic twist that resulted in the maximum thrust is compared.

Results from the model can be usefully compared to the efficiencies measured from motor-driven rowing and flapping appendages. A motor driven rowing fin with a fan-shaped planform had a maximum $\eta = 0.1 – 0.15$ at $k = 2$ (Kato 1999) compared to $\eta = 0.09$ and 0.04 for our feathered and twisted rowing appendages at $k = 2$ (Figure 2*b*). A motor driven flapping wing that passively twisted along its span had a η in the range 0.1 to 0.5 (Archer *et al*. 1979). Importantly, their empirical data fit a theoretical model they developed whose results can be more easily compared to the data presented here. For the Archer et al. model, peak $\eta = 0.65$ occurred at $k = 0.21$ and with a twist amplitude of 40° at the distal tip. By comparison, the peak $\eta = 0.59$ of our flapping model occurred at $k = 0.18$ and a twist amplitude of 48°. Given these comparisons, we believe our simple, blade-element model is quite sufficient to evaluate rowing vs. flapping performance.

How do our results compare with estimates of mechanical efficiency of rowing and flapping animals? Using oxygen consumption data, Webb (Webb 1974) found $\eta = 0.6 - 0.65$ for the flapping stroke of the surfperch, *Cymatogaster aggregata* swimming at $k = 0.25$. For our model flapping appendage, we found a peak $\eta = 0.58$ at $k = 0.25$ (Figure 2*b*).

Performance trade-offs: efficiency vs. maneuverability

The higher η of the flapping appendage suggests that animals that need to cruise at some constant speed for prolonged periods should employ a flapping gait. Sea turtles, which can both row their hind limbs and flap their forelimbs, migrate hundreds to thousands of kilometers between foraging and nesting areas (Wyneken 1997). Available field observations indicate that adult green turtles and loggerheads employ a flapping geometry exclusively for these migrations (Wyneken 1997). Of the many semiaquatic and aquatic mammals that propel themselves with oscillating appendages, only species that flap their appendages, the fur seals and sea lions (Otariidae) (Feldkamp 1987a; Feldkamp 1987b), make aquatic migrations (Riedman 1990).

Blake (Blake 1979; Blake 1980; Webb & Blake 1985) has suggested that rowing propulsion is more efficient than axial propulsion at slow speeds and should be the preferred gait for slow speed swimming and maneuvering. But why not flap at low speeds, given that flapping is less costly than rowing at all speeds? At low speeds, rowing does generate more thrust than flapping (this paper and Vogel, 1994). For cruising at low speeds, however, low thrust production should not handicap a flapping appendage since it can simply oscillate at a higher frequency and still be more energetically efficient than the rowing appendage.

But slowly swimming animals do not generally swim at uniform speeds. Instead, slowly swimming animals frequently accelerate forwards, turn and brake. These behaviors are facilitated by large thrust or drag generated by the paired appendages. This suggests that limb design for animals that prefer to swim at slow speeds are constrained by a performance trade-off. To maximize energy efficiency, flapping appendages are most effective. To maximize maneuverability, rowing appendages are most effective. Maneuvering performance should be related more to the force generated during the power stroke and not averaged over both strokes. We found the advantage of the rowing fin for generating thrust at slow speeds increased sharply after considering only the power stroke (Figure 2*d*).

These results suggest that rowing should be associated with slow speed swimming and especially maneuvering whereas flapping should be associated with the ability to achieve high swimming speeds (Vogel 1994). Indeed, many fishes row with their fins for slow speed swimming and maneuvering but switch to axial undulation to achieve higher speeds (Webb 1993, 1994). The highest pectoral-fin powered speeds are achieved in species of Acanthuridae (surgeonfishes), Pomacentridae (damselfishes), Scaridae (parrotfishes), Embiotocidae (surfperches) and Labridae (wrasses) that flap the pectoral fins (Walker & Westneat 1997; Webb 1993; Webb 1994; Westneat & Walker 1997).

Data from turtles also support the predictions of the model. Limited laboratory comparisons of marine and freshwater turtles indicate that the green sea turtle, *Chelonia mydas,* reached a maximum speed of approximately 13 $BL \cdot s^{-1}$ using flapping foreflippers (Davenport & Pearson 1994). By

contrast, the freshwater turtle *Mauremys caspica* attained a top speed of about 2.2 BL/s using simultaneous fore and hind limb rowing (Davenport & Pearson 1994).

Additionally, available data show that nearly all sea turtles, at least as post-hatchlings and juveniles, switch gaits to achieve faster speeds. During their pelagic phase, sea-turtles tend to swim slowly at the surface using hind-limb rowing strokes but switch to a forelimb flapping gait for escape behaviors (Davenport *et al*. 1997; Davenport & Pearson 1994; Wyneken 1997). By contrast, post-hatchling sea turtles predominantly employ a flapping stroke at the onset of relatively high-speed, offshore migrations (Wyneken 1997).

This study demonstrates the value of combining comparative studies with experimental models that address the causal relationship between phenotype and performance. Despite the wide range of variables influencing locomotor ability, the simulations of aquatic flight in this study suggest specific functional roles for flapping and rowing fins. Modeling approaches based upon realistic biological parameters form the cornerstone of attempts to explain the vast diversity in structure and function for aquatic locomotion. We examine several flapping and rowing fishes to examine the predictions of this model with living coral reef fishes.

Testing the Model: Fin Shape, Performance and Behavior in Reef Fishes

A central goal of bioengineering in the field of underwater vehicle design is to understand mechanisms of propulsion, the structure of propulsors, and the performance levels that biological propulsors give to living animals. Below, we present data on fin shape, swimming performance from flow tank trials, and key features of fin stroke behavior that determine the degree of rowing or flapping during swimming. We studied four species that varied in fin shape and swimming style: the bird wrasse (*Gomphosus varius*), the slippery dick (*Halichoeres bivittatus*), the red-finned wrasse (*Cirrhilabrus rubripinnis*) and the eight-lined wrasse (*Pseudocheilinus octotaenia*).

Fin Morphometrics. Fins of 10 *G. varius* (10.5-16.9 cm TL), 9 *H. bivittatus* (11.8-18.1 cm TL), 6 *C. rubripinnis* (7.3-8.0 cm TL), and 8 *P. octotaenia* (7.7-10.1 cm TL) were removed and pinned to a foam board with fin rays in an expanded (splayed) position, and brushed with full strength formalin to preserve them in this position. Digital images of the fins were then captured using a Wild M3Z stereomicroscope equipped with a Kodak DC120 digital camera. Digital images were then saved in Photoshop 4.0 and duplicated as TIFF format files for analysis using NIH Image 1.62 on a Macintosh G3 computer.

Fin semispan, R, was measured by the length of the leading edge fin ray (Fig. 3A, chord between landmarks 1 and 2). Assuming bilateral symmetry, fin Aspect Ratio, AR, was computed as $AR = 2R^2/A$, where A is the area of the pinned fin. A measure that reflects whether a fin is distally expanding or tapering is the distribution of spans from leading to trailing edge. The fin base and distal edge were divided into five equal parts, lines through corresponding points were constructed, and the segments, or spans, between the ray base and ray tips were measured (Fig. 3B). These spans were standardized by the square root of A.

Five curved chords were constructed at equal intervals along the span. The most proximal curved chord is the base of the fin rays (Fig. 3C). Importantly, every point along one of the distal curved chords has an equal distance, r_j, from the basal chord (Fig. 3C). Because forces and torques of an oscillating fin are a function of the distance from the fin base, we measured these curved chords instead of the more traditional straight chords.

A pair of curved chords bounds a fin element, e_j, with area, a_j, that is approximately $\Delta r(c_j + c_{j+1})/2$, where Δr is $R/5$ and c_j is the length of the jth constructed chord (Fig. 3C). Note that $(c_j + c_{j+1})/2$ is the mean chord for element j. Because the fifth (most distal) element is not bounded by a distal chord, we used the measured area of the element for a_5. The mean chord for the fifth element is $a_5/\Delta r$. Following Ellington (1984), we standardized areas by $\hat{a}_j = \frac{a_j}{A}$. The standardized kth moment of area is $\sum_{j=1}^{5} \hat{r}_j^k \hat{a}_j$, where $\hat{r}_j = \frac{r_j - \Delta r}{R}$. The first moment of area is the relative distance of center of fin area from the fin base and generally indicates if the fin is paddle-shaped (distally expanding) or wing-shaped

(distally tapering). The 2nd moment of area is proportional to aerodynamic (Weis-Fogh, 1973) and inertial (including the acceleration reaction) forces. The third moment of area is proportional to mean profile power (Weis-Fogh, 1973).

Fin shape results. Aspect ratio in the four species ranged from about 1.5 in *P. octotaenia* to 3.5 in *G. varius* (Table 1; Fig. 4A). As expected, AR in *G. varius* was significantly greater than in *H. bivittatus* ($F = 42.5$, $P < 0.0001$) and that in *C. rubripinnis* was significantly greater than in *P. octotaenia* ($F = 156.6$, $P < 0.0001$).

The distribution of relative fin spans (span over square root of area) from leading to trailing edge was also different among species (Fig. 5A). The leading edge (completed by the second fin ray) is longest in *C. rubripinnis* and *G. varius* while a more caudal span is longest in *H. bivittatus* and *P. octotaenia* (Fig. 5A). The pattern of loadings on the first canonical variate of the spans data indicates that the major axis of shape difference among the four species reflects a contrast between the relative lengths of the anterior and posterior spans (Table 2). Scores on the first canonical variate (Fig. 4B) show that both *G. varius* and *C. rubripinnis* have long anterior spans relative to the posterior spans, *P. octotaenia* has short anterior spans, and *H. bivittatus* has relatively intermediate anterior spans. Scores on the first canonical variate significantly differ between *G. varius* and *H. bivittatus* ($F = 85.5$, $P < 0.0001$) and between *C. rubripinnis* and *P. octotaenia* ($F = 649.7$, $P < 0.0001$).

The fins of *G. varius* and *C. rubripinnis* taper substantially (that is, chord lengths decrease) distal to the 3rd chord while the fin of *H. bivittatus* tapers only distal to the fourth chord and the fin of *P. octotaenia* fails to taper at all (Fig. 5B). This variation in shape is reflected in the first through third moments of area (Table 1). The first moment (or center) of area is nearer the fin base in *G. varius* and *C. rubripinnis*, nearer the distal edge in *P. octotaenia* and has a more intermediate location in *H. bivittatus* (Table 1, Fig. 4C). The first moment differs significantly between *G. varius* and *H. bivittatus* ($F = 27.6$, $P < 0.0001$) and between *C. rubripinnis* and *P. octotaenia* ($F = 379.8$, $P < 0.0001$) (Fig. 4C).

Performance trials and kinematic variables

We used an open-top, circular flow tank for all swimming trials. Water temperature in the flow tank was maintained at 25 ±1° C. We placed a plexiglass half-pipe into the main section that proved effective at forcing the fish to swim in the water column. To avoid negative physiological responses to the tank, prior to each trial, we piped water from one of the reservoirs of the main system into the flow tank. Following each trial, all water from the flow tank was pumped back into the system.

We used an increasing velocity test to measure critical swimming speed, U_{crit}, which is the maximum speed that can be maintained for a set length of time and is often used as a proxy of the maximum sustained swimming speed (Hammer, 1995). All fish were tested individually to avoid interactions that could reduce performance. A trial ended when the fish could not be stimulated to regain position in the water. The flow speed at which the individual could not maintain position with only pectoral fin propulsion was noted (U_{pc}, Drucker, 1996).

Prior to placement in the flow tank, total Body Length (BL), measured from the tip of the snout to the posterior margin of the caudal fin, was estimated to the nearest 0.5 cm. Fish acclimated to the flow tank for one hour. Following the rest period, we slowly increased water speed to the initial velocity. In general, the initial velocity was 2 $BL \cdot s^{-1}$. We increased the flow speed at constant increments, relative to body length, at 15 minute intervals. For all *G. varius* and *H. bivittatus*, increments were 0.25 $BL \cdot s^{-1}$. Because of their smaller body size, most of the *C. rubripinnis* and *P. octotaenia* increments were 0.33 $BL \cdot s^{-1}$ although we did use 0.25 $BL \cdot s^{-1}$ increments for some trials. We used 15 minute intervals, above the minimal amount of time necessary to avoid an inflated U_{crit} (Hammer, 1995).

We measured the maximum speed, $U_{p\text{-}max}$, that an individual could achieve using only labriform propulsion. To measure $U_{p\text{-}max}$, we used an increasing velocity test in which the speed of the flow was increased approximately 2.2 $cm \cdot s^{-1}$ once it was determined if the individual could maintain position over several fin beat cycles by using only the pectoral fins to generate thrust. $U_{p\text{-}max}$ was taken as the final speed prior to the speed at which the individual failed to maintain position.

Table 1. Fin shape data for four species of labrid fishes. Means and standard deviations (in parenthesis) are given. TL (Total fish length) is in millimeters. AR is aspect ratio; S1 is the leading edge span relative to root fin area; S6 is the trailing edge span relative to root fin area; C1 is the mean chord of the first (proximal-most) element relative to mean chord of fin; C1is the mean chord of the fifth (distal-most) element relative to mean chord of fin; M1, M2, M3 are the standardized first, second and third moments of fin area.

Species	***G. varius***	***H. bivittatus***	***C. rubripinnis***	***P. octotenia***
Variable	***n=10***	***n=8***	***n=6***	***n=7***
TL	133.50 (21.69)	144.56 (22.98)	77.00 (3.69)	88.00 (7.17)
AR	3.49 (0.3)	2.34 (0.46)	2.94 (0.25)	1.52 (0.18)
S1	1.32 (0.06)	1.08 (0.11)	1.21 (0.05)	0.87 (0.05)
S6	0.50 (0.05)	0.65 (0.05)	0.57 (0.07)	0.60 (0.05)
C1	0.78 (0.10)	0.60 (0.06)	0.85 (0.05)	0.47 (0.05)
C5	0.55 (0.12)	1.23 (0.43)	0.41 (0.08)	2.21 (0.19)
M1	0.47 (0.03)	0.59 (0.07)	0.46 (0.02)	0.71 (0.03)
M2	0.28 (0.02)	0.40 (0.06)	0.26 (0.01)	0.53(0.03)
M3	0.19 (0.02)	0.30 (0.06)	0.17 (0.01)	0.43 (0.05)

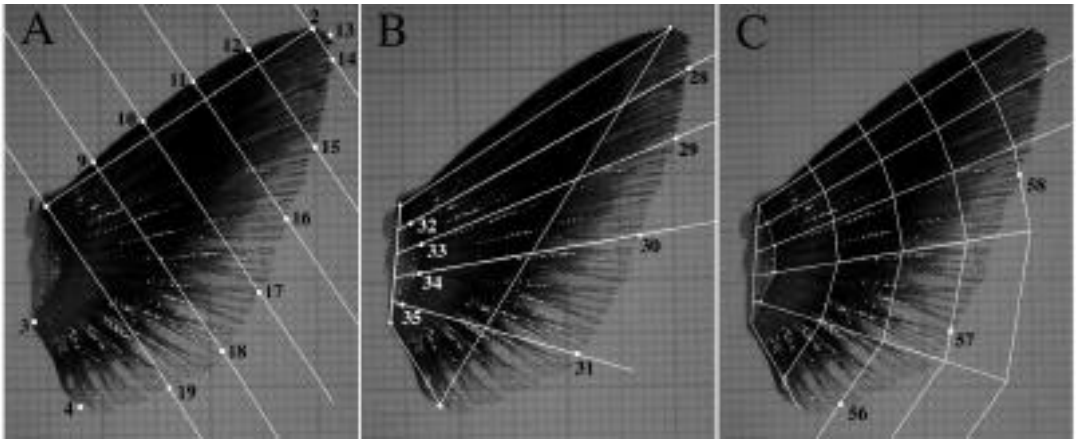

Figure 3. Morphometrics of fin shape. (A) Landmarks used to compute fin area. (B) Spans, $S_1 = S_6$, measured as the length from the base of the fin ray base to the fin ray tips. (C) Curved chords. The area of the elements, e_j, bounded by the chords was used to estimate the moments of area.

Prior to placement in the flow tank, total Body Length (BL), measured from the tip of the snout to the posterior margin of the caudal fin, was estimated to the nearest 0.5 cm. Fish acclimated to the flow tank for one hour. Following the rest period, we slowly increased water speed to the initial velocity. In general, the initial velocity was 2 BL•s^{-1}. We increased the flow speed at constant increments, relative to body length, at 15 minute intervals. For all *G. varius* and *H. bivittatus*, increments were 0.25 BL•s^{-1}. Because of their smaller body size, most of the *C. rubripinnis* and *P. octotaenia* increments were 0.33 BL•s^{-1} although we did use 0.25 BL•s^{-1} increments for some trials. We used 15 minute intervals, above the minimal amount of time necessary to avoid an inflated U_{crit} (Hammer, 1995).

We measured the maximum speed, $U_{p\text{-}max}$, that an individual could achieve in the flow using only labriform propulsion. To measure $U_{p\text{-}max}$, we used an increasing velocity test in which the speed of the flow was increased approximately 2.2 cm•s^{-1} once it was determined if the individual could maintain position over several fin beat cycles by using only the pectoral fins to generate thrust. $U_{p\text{-}max}$ was taken as the final speed prior to the speed at which the individual failed to maintain position.

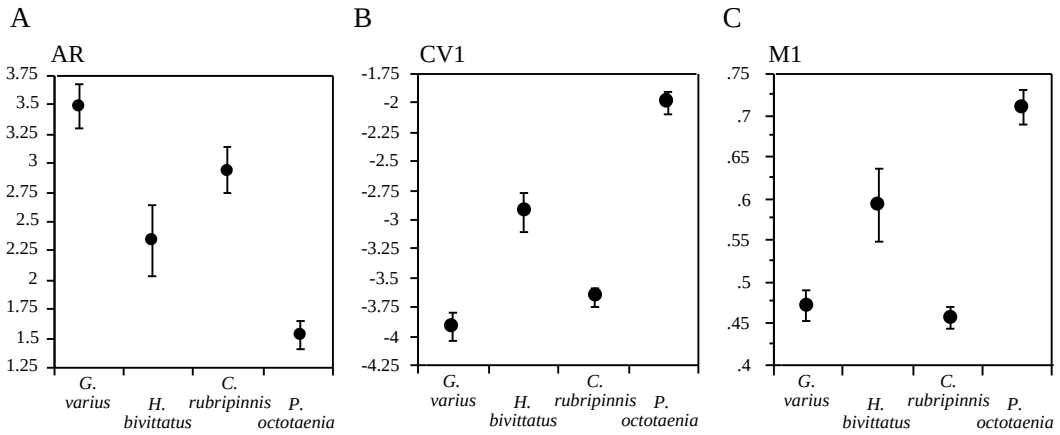

Figure 4. Distribution of composite functional shape variables. (A) Aspect ratio of the pectoral fin. (B) First canonical variate of size-standardized span data. (C) First standardized moment of area (relative distance of center of fin area from fin base) of pectoral fins. Bars in A-C are 2 standard errors.

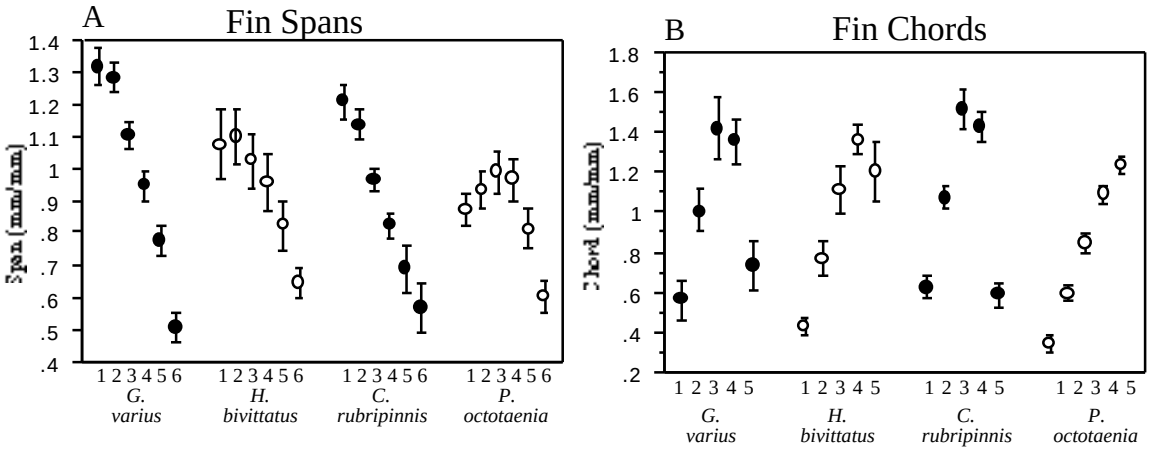

Figure 5. Span and chord distributions of pectoral fin. (A) Mean of spans standardized by root fin area. The spans are ordered (1-6) from leading to trailing edge. (B) Means of curved chords standardized by mean curved chord. The chords are ordered (1-5) from proximal to distal. Bars are one standard deviation.

Following recovery from the increasing velocity test, fish were filmed swimming at a range of speeds in the flow tank following the protocol in Walker & Westneat (1997). Fin beats were digitized using a modification of the public domain NIH Image program. From the digitized sequences, five kinematic variables were constructed: frequency of the stroke cycle, stroke angle, stroke plane angle, abduction angle and adduction angle.

The stroke angle, ϕ, is the maximum angular displacement of the leading edge ray over the fin beat. ϕ was measured as the angle between the three-dimensional vectors representing the position of the distal tip of the leading edge ray, with its base at the origin, at maximum adduction and maximum abduction. Because the data were digitized from a two-dimensional lateral view, the coordinates of the third dimension had to be reconstructed. The *x* (dorsoventral) and *z* (mediolateral) axes were aligned with the horizontal and vertical axes, respectively. At maximum adduction (positioned back against the body), it was assumed that the fin ray was in the *xz* plane (i.e. $y = 0$) and the length of the ray was computed. At maximum abduction, the y component was estimated from the length of the ray and the digitized *x* and *z* components.

The stroke plane angle, β, is the angle between the path of fin movement in the *xz* plane and a unit **z** (or dorsoventral) vector

(Jensen, 1956). Following Walker & Westneat (1997), we use the slope, *b*, of the major axis of the path of the tip of the leading edge ray to describe the slope of fin movement. β is then found by $\beta = \pi/2 - \tan^{-1}(b)$. Prior to computing β, the digitized points were smoothed with a quintic spline (Walker, 1998) and interpolated to 100 points using the software QuicKurve (Walker, 1998).

The abduction and adduction strokes were not swept out on the same plane; the abduction stroke plane was always steeper than the adduction stroke plane. That is, during abduction, the fin tended to sweep down while during adduction, the fin tended to sweep back. We therefore computed separate stroke plane angles for the abduction and adduction strokes. We refer to these as the down and up stroke plane angles. The down and up stroke planes were estimated by the line segment in the *xz* plane spanning the points that were 25% and 75% of the distance along the abduction or adduction curve. Down and up stroke angles were computed as the angle between these line segments and the unit **z** vector.

Results: Kinematics and Performance

The stroke plane angle, β, decreased significantly (became steeper or more dorso-ventral) with speed in *H. bivittatus* (P≤0.0001) and *P. octotaenia* (P≤ 0.0001) but not in *G. varius* (P=0.24) or *C. rubripinnis* (P=0.0645). Downstroke plane angles decreased significantly with speed in all four species (*H. bivittatus*: P≤0.0001; *G. varius* : P=0.0044; *P. octotaenia*: P≤0.0001; *C. rubripinnis* : P=0.0393), although the magnitude of the decrease was much less in *G. varius* and *C. rubripinnis* (Fig. 6, Table 2). The upstroke plane angle decreased significantly with speed in all species but *G. varius* (*H. bivittatus*: P≤0.0001; *G. varius* : P=0.344; *P. octotaenia*: P=0.0009; *C. rubripinnis* : P=0.028) but the magnitude of the change was much less in *C. rubripinnis* than in either *H. bivittatus* or *P. octotaenia* (Fig. 6, Table 2).

We were able to measure stroke plane angles at lower speeds in *H. bivittatus* and *P. octotaenia* than in *G. varius* or *C. rubripinnis.* At the lowest speed measured for *G. varius* (1.42 BL•s^{-1}), *H. bivittatus* had significantly shallower stroke plane, downstroke and upstroke angles than *G. varius* (Fig. 6, Table 2). Similarly, *P. octotaenia* had significantly shallower stroke plane, downstroke and upstroke angles than *C. rubripinnis* at the lowest swimming speeds.

The maximum speed at which kinematic data were measured for both *H. bivittatus* and *G. varius* was 4.3 BL•s^{-1}, which is above the expected Ucrit for even the smallest *H. bivittatus* individuals (Fig. 6; Table 2). At this relative speed, the stroke plane and downstroke angles were significantly shallower in *H. bivittatus* but the upstroke angle was not (Fig. 6, Table 2). The maximum speed at which kinematic data were measured for *P. octotaenia* was 3.9 BL•s^{-1}, only 0.1 BL•s^{-1} less than the mean Ucrit for this species (Table 2). At this speed, the stroke plane, downstroke, and upstroke angles were significantly shallower in *P. octotaenia* than in *C. rubripinnis* (Fig. 6, Table 2).

The stroke angle increased with speed in all species (*H. bivittatus*: P=0.049; *G. varius*: P=0.003; *P. octotaenia*: P≤0.0001; *C. rubripinnis* : P≤0.0001). *H. bivittatus* had a larger stroke angle than *G. varius* at low swimming speeds but no differences occurred at high swimming speeds (Fig. 6, Table 2). By contrast, the stroke angles of *P. octotaenia* and *C. rubripinnis* did not differ at low swimming speeds but the stroke angle of *P. octotaenia* was greater than *C. rubripinnis* at high speeds.

Oscillation frequency increased in all four species (*H. bivittatus*: P≤0.0001; *G. varius* : P≤0.0001; *P. octotaenia*: P≤0.0001; *C. rubripinnis* : P≤0.0001). Frequency did not differ between *H. bivittatus* and *G. varius* at either low or high speeds (Fig. 6, Table 2). *C. rubripinnis* had much greater frequencies than *P. octotaenia* at low speeds (1 BL•s^{-1}) but this difference vanished near the critical swimming speed of *P. octotaen*ia (3.9 BL•s^{-1}).

Critical swimming speeds (Table 3, Fig. 7) increased with body length in both *H. bivittatus* (U_{crit} = 20.7 + 1.95•BL, P=0.03) and *G. varius* (U_{crit} = 0.346 + 5.23•BL, P=0.003). *Up-max* increased with body length in *G. varius* (*Up-max* = 34.9 + 2.1•BL, P=0.03) but not *H. bivittatus* (P = 0.24). *G. varius* had higher critical swimming speed than *H. bivittatus* at the longest but not smallest body lengths (Table 3, Fig. 7). *G. varius* was able to reach higher *Up-max* than *H. bivittatus* at all body lengths (Table 3, Fig. 7). *C. rubripinnis* had significantly higher U_{crit} ($P \leq 0.0001$) and *Up-max* ($P \leq 0.0357$) than *P. octotaenia* (Fig. 7).

Table 2. Kinematic comparisons across speed range. Stroke plane angles for entire stroke (β) and for each half-stroke independently (βdown and βup) are shown. The angles are between the projection of the stroke plane onto the sagittal (xz) plane and the dorsoventral (z) axis. 2Φ is the stroke angle (twice the stroke amplitude). *f* is the stroke frequency.

	BL/s	*H. bivittatus*	*G. varius*	P
β (°)	1.4	36.2	16.7	≤0.0001
	4.3	22.4	16.7	0.034
β_{down} (°)	1.4	26.2	10.2	≤0.0001
	4.3	12.5	2.7	0.0108
β_{up} (°)	1.4	44.6	23.3	0.0001
	4.3	31.4	23.3	0.172
2Φ (°)	1.4	110.4	91.1	0.0003
	4.3	119.2	120.1	0.2748
f (Hz)	1.4	3.7	3.3	0.5067
	4.3	5.4	4.6	0.3847
	BL/s	*P. octotaenia*	*C.rubripinnis*	P
β (°)	1	47.2	22.4	0.0002
	3.9	30.1	22.4	0.0008
β_{down} (°)	1	36.8	12.6	0.0006
	3.9	14.2	9.4	0.0109
β_{up} (°)	1	56.5	33.1	0.0002
	3.9	41.4	29.3	0.007
2Φ (°)	1	91.9	89.8	0.2764
	3.9	134.3	113.8	0.0019
f (Hz)	1	3.1	6.4	0.0024
	3.9	7.9	8.9	0.065

Table 3. Critical swimming speed (*Ucrit*) and maximum pectoral-powered speed (*Up-max*) at the high and low end of the size range (TL, total length) for *Gomphosus varius* and *Halichoeres bivittatus*, and for sampled individuals of *C. rubripinnis* and *P. octotaenia*.

	TL	*H. bivittatus*	*G.varius*
Ucrit	9	38.2	47.4
	16	52.0	84.0
Up-max	12	35.5	60.1
	17	37.5	70.6

	TL	*C. rubripinnis*	*P. octotaenia*
Ucrit	8.1	49.0	
	9.2		37.3
Up-max	8.1	61.7	
	9.2		27.9

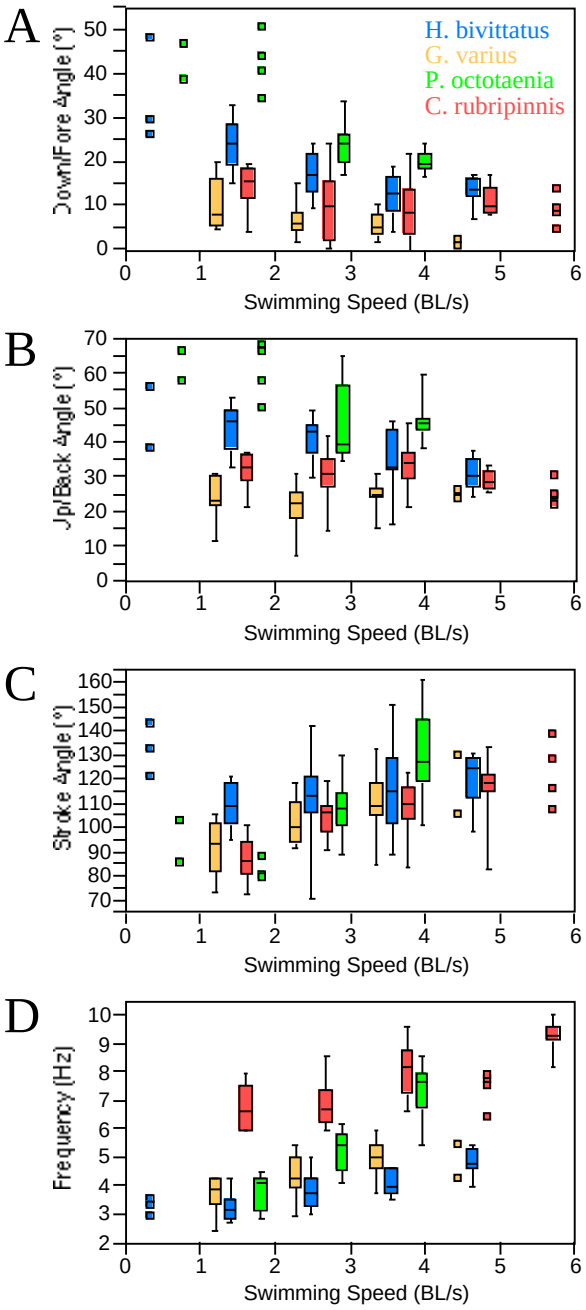

Figure 6. (A-D) Kinematic changes with swimming speed in four labrid species. Box and whiskers represent distribution of the variable for the species. The median of the distribution is the line within the box. The 25th and 75th percentiles are represented by the top and bottom box edges. The 10th and 90th percentile are represented by the caps on the vertical lines (whiskers) outside of the box. Small samples are represented by a square box.

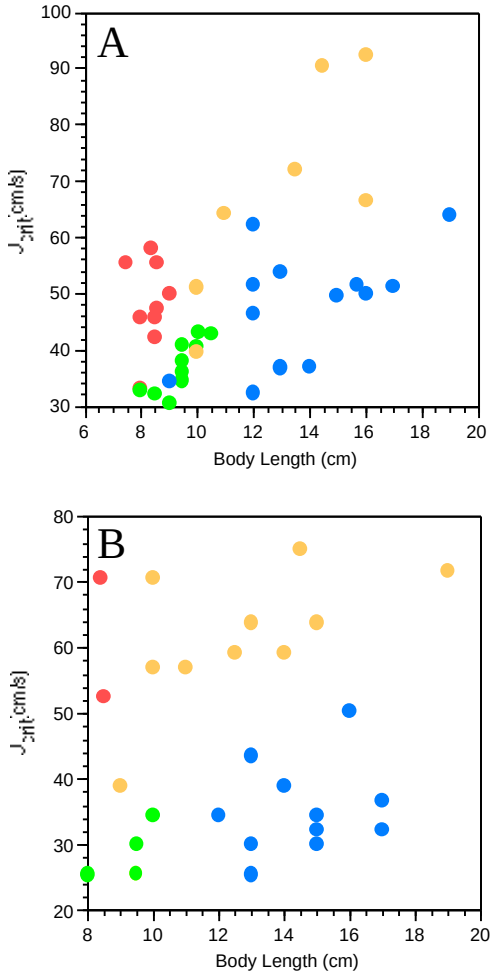

Figure 7. (A) Critical swimming speed, U_{crit}, and (B) maximum pectoral fin powered speed, $U_{p\text{-}max}$, for the individuals of the four labrid fishes.

We also noted the speed at which fish began to rely on intermittent, axial kicking to regain position. Drucker & Jensen (1996) referred to this speed as *Upc*. Intermittent axial kicking augmented the critical swimming speeds of some species above what could be maintained with the pectoral fins working alone. The mean *Ucrit – Upc* was 9.1% in *H. bivittatus*, 0.0% in *G. varius*, 12.4% in *P. octotaenia*, and 3.7% in *C. rubripinnis*.

The trend of increasing critical swimming speed with body length in BCF propulsors is similar to that within the wrasses (Fig. 8). A least squares regression through the BCF propulsor data (Fig. 8) shows the expected *Ucrit* of BCF propulsors as a function of size ($\hat{U}_{exp\text{-}BCF}$). Expected *Ucrit*s values for the wrasses in this study suggest that wrasses that flap their pectoral fins have critical swimming speeds that are greater than $\hat{U}_{exp\text{-}BCF}$ while wrasses that row have critical swimming speeds that are less than $\hat{U}_{exp\text{-}BCF}$ (Fig. 8).

DISCUSSION

A major goal of our research is to understand the functional basis of performance variation among fishes swimming in the labriform mode. This variability in performance and the factors that control it (fin shape, motion, and hydrodynamics) may be of use to the engineer searching for biological answers to machine design questions. Our results identify morphological design correlates of cruising performance. High speed, high endurance species had tapered, high aspect ratio pectoral fins that articulated with the body at low angles relative to the two species with lower speed and lower endurance. Additionally, we found that fishes designed to have a more flapping stroke can achieve and maintain higher swimming speeds than fishes designed for a rowing stroke. However, the difference between stroke geometry at fatigue velocities varies only slightly between fishes with the two different designs. Finally, we found that labrid fishes, which swim to fatigue employing the paired pectoral fins, have size-specific critical swimming speeds expected of fishes swimming with axial undulatory gaits.

Mechanical design and fin shape

Fin shape varies with kinematics and swimming performance as predicted by models of fin function. Aspect ratio is highest and first moments of area are lowest in *G. varius* and *C. rubripinnis*, the two species with the most vertical stroke plane and the two that can achieve and maintain the highest pectoral fin powered swimming speeds. The size-specific first moment of area and the first canonical variate of the size-specific span data are measures of static fin shape; specifically, the degree to which a fin is wing-shaped (tapers distally) or paddle shaped (expands distally). Fishes are able to actively control the spread of the fin rays and the shape of the active fin is most relevant to its function. Nevertheless, the shape of an oscillating fin is limited by features of the fin that we measured: aspect ratio, fin chords, and spans.

Among pectoral swimmers in fishes, *H.*

bivittatus and *P. octotaenia* have a pectoral fin that is intermediate between that of an exclusive rower (the stickleback, *G. aculeatus*) and the exclusive flappers (*G. varius* and *C. rubripinnis*). The range of motions observed in *H. bivittatus* and *P. octotaenia* may allow these fish to match functional requirements for reasonable steady swimming performance with the need for a more efficient or more effective stroke. For example, a stroke with a shallow stroke plane should be able to generate large fore-aft forces without large lift, promoting rapid, pectoral-fin powered starts, stops, and lateral turns. A shallow stroke plane might also facilitate the ability to hover. While *H. bivittatus* and *P. octotaenia* hover easily, *G. varius* must pitch its body upward at a large angle in order to hover for a short duration, a behavior that mimics that of many insects Dudley (2000). In this position the fins are effectively rowing. With increased swimming speed, the steeper stroke plane should allow the fish to generate large enough forces to balance the increased parasite drag.

Gait changes, performance, and efficiency.

All four species progressed through a series of gait changes from slow to high speed swimming. At slow cruising speeds, *P. octotaenia* and *C. rubripinnis* employed a combination of pectoral fin oscillation and dorsal fin undulation while *H. bivittatus* and *G. varius* employed only a labriform mode. At moderate to near peak speeds, all four species used only the pectoral fins. At the extreme fatigue velocity, all four species employed a burst and flap gait, that is, they alternated between bursts of axial undulation and labriform propulsion.

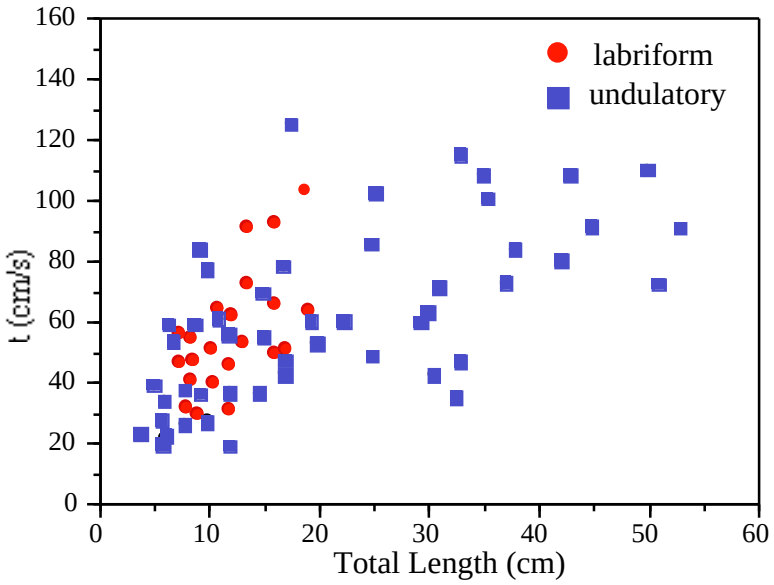

Figure 8. Critical swimming speed, *Ucrit* performance of labriform swimmers compared to the performance of fishes swimming by undulatory body-and-caudal fin (BCF) propulsion.

Many structural and physiological factors can account for performance differences among species. We used our previous work on simulated fins to make a precise prediction between one aspect of fin kinematics and performance. Specifically, we expected swimming performance to vary with stroke plane angle. In order to reject the possibility that performance differences were simply a function of either stroke angle or frequency, however, we also measured these variables in all four species. Swimming speed should increase with both frequency and amplitude of the fin stroke. At the fatigue velocities of the rowers, however, no difference occurred between the stroke angle of *H. bivittatus* and *G. varius*, the stroke angle of *P. octotaenia was greater* than that for *C. rubripinnis*, frequencies *were greater* in *H. bivittatus* than in *G. varius*, and no differences in frequency were observed between *P. octotaenia* and *C. rubripinnis*. These results suggest that stroke

angle and cycle frequency cannot account for the superior swimming performance of *G. varius* and *C. rubripinnis.*

Can the stroke plane angle explain the performance difference? The two species classified *a priori* as flappers had significantly higher U_{crit}s and $U_{p\text{-}max}$s than the two species classified as rowers, which supports the hypothesis that fishes that flap their fins should be able to maintain higher pectoral-fin-powered swimming speeds than fishes that row. Interestingly, however, while the dynamic shape of the fin stroke differed greatly between rowers and flappers at slow speeds, at speeds near fatigue velocities the angles of fin motion differed by only 5°-12°. More specific physical or virtual models of fin oscillation could determine if this small difference in upstroke and downstroke angles can account for performance differences between the rowers and flappers

Is the decrease in stroke plane angle with increasing swimming speeds in *H. bivittatus* and *P. octotaenia* (Fig. 6) necessary for increased thrust generation or is it a strategy to maintain high mechanical efficiency across a broad range of speeds? Walker & Westneat (2000) showed that a flapping stroke is much more mechanically efficient than a rowing stroke across all swimming speeds, which suggests that the change in stroke plane angle is necessary for increased thrust generation.

There are two basic ways that a pair of rowing fins can modify their dynamic shape to generate the increased thrust necessary to balance parasite drag as swimming speed increases: the amplitude and/or frequency can increase enough to maintain a thrust component of the net force during adduction or they can oscillate with a vertical component to generate additional thrust during abduction. A fin abducting with a downward component generates lift in addition to thrust. Confining the vertical motion to abduction produces a net lift over the stroke cycle. Negatively buoyant fish could potentially use this stroke geometry to compensate the downward force on the body. For neutrally buoyant fish, adducting the fin with the appropriate upward component will produce zero net lift.

Because the horizontal component of the local flow increases with speed, a fin abducting with a shallow stroke plane angle must increase its cycle frequency and steepen its stroke plane to maintain thrust generation at increasingly higher swimming speeds. This is essentially how many insects control the stroke plane angle from slow to fast forward flight (Dudley, 2000). *H. bivittatus* and *P. octotaenia* also appear to employ this strategy. In contrast, a decrease in stroke plane angle with increasing swimming speed is not necessary for fishes with fins that always oscillate with steep stroke planes. Instead, these flapping fins can generate more thrust simply by simultaneously increasing cycle frequency and the magnitude of the pitch of the fin chords. *G. varius* and probably *C. rubripinnis* employ this alternative strategy. The diversity of fin designs in fishes make this an excellent group for examining alternative strategies for achieving high swimming performance.

Given that the flapping gait is more mechanically efficient than the rowing gait at all speeds (Walker and Westneat, 2000), why do *H. bivittatus* and *P. octotaenia* not flap their fins at low speeds? The pectoral fins of *H. bivittatus* and *P. octotaenia* appear designed for the wide range of motions between rowing and flapping. For example, the more vertical articulation of the pectoral fin, relative to that of the *G. varius* and *C. rubripinnis,* should facilitate a more fore-aft motion. Additionally, the pectoral fin of the rowers is relatively broad distally, a shape that has been shown to improve the performance of a rowing fin (Blake, 1979). The kinematic and morphological data, then, suggest that *H. bivittatus* and *P. octotaenia* are labriform swimming generalists, and may be able to exploit advantages of both rowing and flapping, but at some cost to cruising performance.

Fin mechanisms for AUV designs

Discussions of pectoral fin swimming in fishes have largely focused on the benefits of the fins during hovering, slow swimming and maneuvering (Breder, 1926; Harris, 1937; Harris, 1953; Webb, 1982, 1984; Blake, 1983; Geerlink, 1989). However, the comparative data in this study show that wrasses swimming with flapping pectoral fins can achieve and maintain swimming speeds higher than $U_{exp\text{-}BCF}$ (Fig. 8). While not as high as that measured for pelagic and anadromous fishes in the comparative sample, the relatively high, pectoral-fin powered U_{crit}s of *G. varius* and *C. rubripinnis* suggest that the loss of axial red

muscle fibers has not limited wrasses to a life in slow motion. Rather, the mechanical design of the fin and the physiology of the pectoral muscles enable labrid fishes to attain comparable swimming speeds and efficiency with a labriform gait.

The high efficiency and performance of the labriform mode of locomotion in fishes suggests that it would be a useful mode of propulsion for autonomous underwater vehicles. Several design features of the fish fin mechanisms might be usefully incorporated into vehicle propulsors. Fin shape is a key determinant of propulsive efficiency, a result made clear from both hydrodynamic simulations and measurements of living animals. Incorporation of fin designs that are intermediate in aspect ratio and area distribution or are capable of changing shape would allow both high efficiency during cruising in nearshore aquatic habitats and high thrust for maneuverability in surge zones or complex three-dimensional environments. Given a particular fin shape, stroke plane angle, camber and twisting of the fin, and stroke amplitude are the central determinants of thrust. Control mechanisms that can mimic the diversity of motions in the fin stroke of a large coral reef fish would provide an AUV with an impressive level of control. Recent and continuing research on neural control of the pectoral fin in coral reef fishes (i.e. Westneat and Walker, 1997) may provide guidance control programs that can create biomimicry of complex fin motions for maximum thrust and maneuverability.

Acknowledgments. This work was funded by Office of Naval Research grant N00014-99-0184 and NSF grant DEB-9815614.

Literature Cited

Archer, R. D., Sapuppo, J. & Betteridge, D. S. 1979. Propulsion characteristics of flapping wings. *Aeronaut. J.* **83**, 355-371.

Blake, R. W. 1979 The mechanics of labriform locomotion I. Labriform locomotion in the angelfish (*Pterophyllum eimekei*): an analysis of the power stroke. *J. Exp. Biol.* **82**, 255-271.

Blake, R. W. 1980 The mechanics of labriform locomotion: analysis of the recovery stroke and the overall fin-beat cycle propulsive efficiency in the angelfish. *J. Exp. Biol.* **85**, 337-342.

Blake, R. W. 1985 Hydrodynamics of swimming in the water boatman, *Cenocorixa bifida*. *Can. J. Zool.* **64**, 1606-1613.

Breder, C. M., Jr. 1926 The locomotion of fishes. *Zoologica* **4**, 159-291.

Daniel, T. L. 1984 Unsteady aspects of aquatic locomotion. *Am. Zool.* **24**, 121-134.

Davenport, J., de Verteuil, N. & Magill, S. 1997 The effects of current velocity and temperature upon swimming in juvenile green turtles *Chelonia mydas* L. *Herp. J.* **7**, 143-147.

Davenport, J. & Pearson, G. A. 1994 Observations on the swimming of the Pacific Ridley, *Lepidochelys olivacea*: Comparisons with other sea turtles. *Herp. J.* **4**, 60-63.

DeLaurier, J. D. 1993 An aerodynamic model for flapping-wing flight. *Aeronaut. J.* **97**, 125-130.

Dickinson, M. H. 1994 The effects of wing rotation on unsteady aerodynammic performance at low Reynolds numbers. *J. Exp. Biol.* **192**, 179-206.

Dickinson, M. H. 1996 Unsteady mechanisms of force generation in aquatic and aerial locomotion. *Am. Zool.* **36**, 537-554.

Dickinson, M. H. & Götz, K. G. 1993 Unsteady aerodynamic performance of model wings at low Reynolds numbers. *J. Exp. Biol.* **174**, 45-64.

Dickinson, M. H. & Götz, K. G. 1996 The wake dynamics and flight forces of the fruit fly *Drosophila melanogaster*. *J. Exp. Biol.* **199**, 2085-2104.

Dickinson, M. H., Lehmann, F.-O. & Sane, S. P. 1999 Wing rotation and the aerodynamic basis of insect flight. *Science* **284**,1954-1960.

Drucker, E. G. and Jensen, J. S. (1996). Pectoral fin locomotion in the striped surfperch. I. Kinematic effects of swimming speed and body size. J. Exp. Biol. **199**, 2235-2242.

Dudley, R. (2000). The Biomechanics of Insect Flight: Form, Function, Evolution. Princeton: Princeton University Press. 476p.

Ellington, C. P., Van den Berg, C. & Willmott, A. P. 1996 Leading-edge vortices in insect flight. *Nature* **384**, 626-630.

Feldkamp, S. D. 1987a Foreflipper propulsion in the California sea lion, *Zalophus californianus. J. Zool., Lond.* **212**, 43-57.

Feldkamp, S. D. 1987b Swimming in the California sea lion: morphometrics, drag, and energetics. *J. Exp. Biol.*

131, 117-135.
Fish, F. E. 1984 Mechanics, power output and efficiency of the swimming muskrat (*Ondatra zibethicus*). *J. Exp. Biol.* **110**, 183-201.
Fish, F. E. 1992 Aquatic Locomotion. In *Mammalian Energetics: Interdisciplinary Views of Metabolism and Reproduction* (ed. T. E. Tomasi & T. H. Horton), pp. 34-63. Ithaca: Cornell University Press.
Fung, Y. C. 1993 *An Introduction to the Theory of Aeroelasticity*. New York: Dover.
Gal, J. M. & Blake, R. W. 1988 Biomechanics of frog swimming. I. Estimation of the propulsive force generated by *Hymenochirus boettgeri*. *J. Exp. Biol.* **138**, 399-411.
Geerlink, P. J. 1989. Pectoral fin morphology: a simple relation with movement pattern? Neth. J. Zool. 39: 166-193.
Harris, J. E. (1937). The mechanical significance of the position and movements of the paired fins in the Teleostei. Papers of the Tortugas Laboratories 31, 173-189.
Hoerner, S. F. 1958 *Fluid-Dynamic Drag*. Midland Park, NJ: Published by the Author.
Hui, C. A. 1988 Penguin swimming. I. Hydrodynamics. *Physiol. Zool.* **61**, 333-342.
Jensen, M. 1956. Biology and physics of locust flight III. The aerodynamics of locust flight. Phil. Trans. R. Soc. Lond. Ser. B 239, 511-552.
Kato, N. 1999 Hydrodynamic characteristics of mechanical pectoral fin. *J. Fluids Eng.* **121**,605-13.
Kuethe, A. M. & Chow, C.-Y. 1986 *Foundations of Aerodynamics*. New York: Wiley & Sons.
Morris, M. J., Gust, G. & Torres, J. J. 1985 Propulsion efficiency and cost of transport for copepods: a hydromechanical model of crustacean swimming. *Mar. Biol.* **86**, 283-295.
Riedman, M. 1990 *The Pinnipeds*. Berkeley: University of California Press.
Thom, A. & Swart, P. 1940 Forces on an airfoil at very low speeds. *J. Roy. Aero. Soc.* **44**, 761.
Vogel, S. 1994 *Life in Moving Fluids (2nd Ed.)*. Princeton: Princeton University Press.
Walker, J.A. 1998. Estimating velocities and accelerations of animal locomotion: A simulation experiment comparing numerical differentiation algorithms. J. Exp. Biol., 201:981-985.
Walker, J. A. & Westneat, M. W. 1997 Labriform propulsion in fishes: Kinematics of flapping aquatic flight in the bird wrasse *Gomphosus varius* (Labridae). *J. Exp. Biol.* **200**, 1549-1569.
Walker, J. A. and M. W. Westneat. 2000. Mechanical performance of aquatic rowing and flying. Proc. Roy. Soc. Lond. B. 267: 1875-81.
Walker, J. A. and M. W. Westneat. 2001. Pectoral fin design and swimming performance in labriform propulsion: A comparison between rowers and flappers. In Press, Journal of Experimental Biology.
Webb, P. W. 1973 Kinematics of pectoral fin propulsion in *Cymatogaster aggregata*. *J. Exp. Biol.* **59**, 697-710.
Webb, P. W. 1974 Efficiency of pectoral fin propulsion of *Cymatogaster aggregata*. In *Swimming and Flying in Nature, vol. 2* (ed. T. Y. Wu, C. J. Brokaw & C. Brennen), pp. 573-584. New York: Plenum.
Webb, P. W. 1993 Swimming. In *The Physiology of Fishes* (ed. D. H. Evans), pp. 47-73. Boca Raton: CRC Press.
Webb, P. W. 1994 Excercise performance of fish. In *Comparative Vertebrate Exercise Physiology: Phyletic Adaptations* (ed. J. H. Jones), pp. 1-49. San Diego: Academic Press.
Webb, P. W. & Blake, R. W. 1985 Swimming. In *Functional Vertebrate Morphology* (ed. M. Hildebrand, D. M. Bramble, K. F. Liem & D. B. Wake), pp. 110-128. Cambridge: Harvard University.
Weis-Fogh, T. 1973. Quick estimates of flight fitness in hovering animals, including novel mechanisms for lift production. J. exp. Biol. 59, 169-230.
Westneat, M. W. 1996. Functional morphology of aquatic flight in fishes: mechanical modeling, kinematics, and electromyography of labriform locomotion. Amer. Zool. 36:582-598.
Westneat, M. W. and J. A. Walker. 1997. Motor patterns of underwater flight: an electromyographic study of the pectoral muscles in the bird wrasse, *Gomphosus varius*. J. Exp. Biol. 200, 1881-1893.
Wyneken, J. 1997 Sea turtle locomotion: Mechanics, behavior, and energetics. In *The Biology of Sea Turtles* (ed. P. Lutz & J. Musick), pp. 165-198. Boca Raton: CRC Press.